Journal of the Optical Society of Korea
Vol. 20, No. 4, August 2016, pp. 500-509

ISSN: 1226-4776(Print) / ISSN: 2093-6885(Online)
DOI: http://dx.doi.org/10.3807/JOSK.2016.20.4.500

Design and Characteristic Measurement of 8000 mm Large Aperture Integrating Sphere

Zhao Zhang[1,2]*, Zhi Wan[1], Xiansheng Li[1], Hongxing Liu[1], Jingxu Sun[1], Zexun Liu[1], Yamin Wang[1,2], Jianwei Ren[1], and Jianyue Ren[1]

[1]Changchun Institute of Optics, Fine Mechanics and Physics, Chinese Academy of Sciences, Changchun 130033, China
[2]University of Chinese Academy of Sciences, Beijing 100049, China

(Received June 15, 2016 : revised July 11, 2016 : accepted July 12, 2016)

Integrating spheres play a central role in the radiometric calibration of remote sensors. With the development of the wide field of view (FOV) remote sensors, aperture diameters of remote sensors are becoming larger and larger. To satisfy the radiometric calibration requirements of full FOV and full aperture, an 8000mm diameter large aperture integrating sphere uniform source with a variable exit port was designed and manufactured. This integrating sphere will be used for pre-launch test and radiometric calibration of remote satellites. In this paper, optical theories were used to design the output spectral radiance. The LightTools software based on ray-tracing simulation method was used to determine the best combination and distribution of inner light sources. A spectral experiment was made to verify the spectral radiance design. To reduce the influence of longtime power-on, a new characteristic measurement method was developed to obtain the radiation characteristic of the integrating sphere, which could greatly improve the measuring efficiency. This method could also be applied to measure other large aperture uniform sources. The obtained results indicate that the spatial uniformity is 98.35%, and the angular uniformity at center position is 98.78%.

Keywords : Radiometric calibration, Large aperture integrating sphere, Simulation, Characteristic measurement
OCIS codes : (120.3150) Integrating spheres; (120.0280) Remote sensing and sensors; (150.1488) Calibration; (120.5630) Radiometry; (350.4800) Optical standards and testing

I. INTRODUCTION

It is well known that uniform source systems provide uniform radiance or irradiance. Their applications include focal-plane array or complete camera test, pixels gain normalization, photographic sensitometry, and remote-observation system calibration [1]. The most common uniform source is the integrating sphere, which is extensively used in high-accuracy radiometric calibration. At present, the standard transfer process of space remote sensing radiometric calibration is: cryogenic absolute radiometer → radiance standard detector → Lambert reflector integrating sphere → space remote sensor. With the increasing requirements of high resolution, large spatial and spectral coverage space-to-earth observation, the optical remote sensing is developing in the direction of wide field of view (FOV), large aperture, and long focal length [2-5]. In this case, radiometric calibration devices need to be large enough to satisfy the calibration requirements of full FOV and full aperture. Hence, the integrating sphere inner diameter and exit port diameter must be developed [6].

Great progress has been made in this field. Nevertheless, when the integrating spheres becoming larger, challenges will be associated with it. There are three important considerations for the large aperture integrating sphere. Firstly, for the use of remote-sensing calibration, the output spectral radiance should satisfy the requirements of the remote sensor's radiometric calibration. Hence, the output spectral radiance is required to be designed before manufacture, especially for the concerned waveband. Secondly, in the application

*Corresponding author: zhangzhao890513@sina.com
Color versions of one or more of the figures in this paper are available online.

of remote-sensing calibration, spatial uniformity and angular uniformity mapping of the integrating sphere are required. Different combinations and distributions of inner light sources could bring about different characteristics of spatial uniformity and angular uniformity. Hence, in the process of design, spatial uniformity and angular uniformity of the integrating sphere should be considered. Finally, as important as the uniformity value, is the method by which uniformity is measured. However, it is not easy to realize the characteristic measurement of a large aperture integrating sphere by the single detector method when its exit port diameter becomes much larger than before. For example, if the exit port diameter is 3200 mm and the mapping interval is 20 mm, then nearly 7.6 hours will be taken to finish the spatial uniformity measurement at each radiance level. Longtime power-on will bring thermal drift, and it is harmful to the inner light sources and sphere coating. As a consequence, results will be inaccurate, and could not evaluate the real characteristics of the integrating sphere.

In this paper, an 8000 mm inner diameter large aperture integrating sphere with a selectable exit port was designed and manufactured. The maximum exit port of the integrating sphere is Φ3200 mm. In Section 2, the integrating design theory and blackbody theory used to design the spectral radiance, the LightTools software used to determine the best combination and distribution of inner light sources basing on ray-tracing simulation method, and the design criterion of large aperture integrating sphere are presented. In Section 3, the theory of characteristic measurement, the single detector method of characteristic measurement, and the restriction of characteristic measurement based on the single detector method are discussed. In Section 4, a newly developed measurement method used to improve measuring efficiency is exhibited, and the consistency algorithm for multiple detectors is explained. In Section 5, the spectral experiment made to verify the spectral radiance design, and the experiment used to measure spatial uniformity and angular uniformity are described. Uncertainty of characteristic measurement is analyzed in Section 6.

II. DESIGN OF LARGE APERTURE INTEGRATING SPHERE

In the application to the radiometric calibration of remote sensors, the spectral radiance of the integrating sphere is required to be designed before manufacture. The spectral radiance produced by an integrating sphere of a given spectral flux input is dependent on the sphere diameter, number of apertures in the sphere or coined aperture fraction area, and the spectral reflectance of the interior coating [8, 9].

$$L_\lambda = \frac{\Phi_\lambda}{\pi A_s} \cdot \frac{\rho_\lambda}{1-\rho_\lambda(1-f)} \tag{1}$$

$$f = \frac{A_p}{A_s} \tag{2}$$

Where L_λ is the sphere coating spectral radiance, ρ_λ is the sphere coating reflectance factor, A_s is the area of the sphere internal surface, A_p is the total area of the integrating sphere exit port, and f is the port fractional area of the integrating sphere. When the input light sources are tungsten halogen lamps, the blackbody radiation theory is applied

$$\Phi_\lambda = \frac{c_1}{\lambda^5} \cdot \frac{1}{e^{c_2/\lambda T}-1} \cdot \frac{\Phi_0}{\sigma T^4} \tag{3}$$

where Φ_λ is radiant flux, c_1 equals 3.7413×10^{-4} W·μm^{-2}, λ is wavelength in microns, c_2 equals 1.4388×10^{4} μm·K, T is the filament temperature in Kelvin, Φ_0 is the lamp rate power, and σ equals 5.6686×10^{-20} W·μm^{-2}·K^{-4}.

In this paper, the Spectraflect material was selected as the sphere coating, whose reflectance is higher than 96% in waveband 0.3~1.2 μm. The reflectance of the Spectralon material is higher than that of the Spectraflect material. However, the Spectraflect material is more suitable for the sphere coating of a large-diameter integrating sphere. This is because the Spectraflect material with spraying technology could be used for large diameter integrating sphere coating processes while the Spectralon material with swaging technology cannot be used. Figure 1 shows the reflectance of the Spectralon material and the Spectraflect material.

This integrating sphere has an internal diameter of 8000 mm conjugated with a variable exit port. The variable diameters of the exit port are 800 mm, 2500 mm, and 3200 mm, which could be selected for the radiometric calibration of different satellite remote sensors. The exit ports of Φ800 mm and Φ2500 mm are shown in Fig. 2.

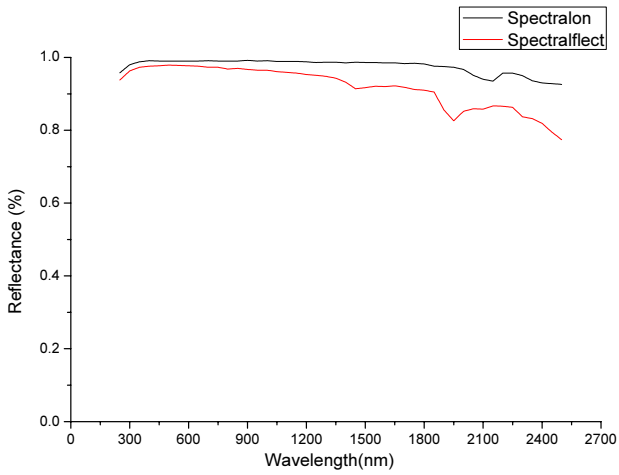

FIG. 1. Reflectance of Spectralon material and Spectraflect material.

The radiation flux and radiance were designed by Eqs. (1)~(3). In common use, the waveband 0.45~0.9 μm is most concerned for the radiometric calibration of optical satellite remote sensors. The radiation flux $\Phi_{0.45\mu m\sim0.9\mu m}$ used for the calibration of optical remote sensors was calculated by Eq. (3). Sequentially the radiance $L_{0.45\mu m\sim0.9\mu m}$ for Φ800 mm exit port was predicted by Eq. (1) and ρ_λ in Fig. 1. In actual use, the waveband 0.45~0.9 μm will be divided into four parts: blue waveband (0.45~0.52 μm), green waveband (0.52~0.6 μm), red waveband (0.63~0.69 μm), and near infrared waveband (0.76~0.9 μm). The integrated radiance was calculated by Eq. (4).

$$L_{\lambda_1\sim\lambda_2}=\int_{\lambda_1}^{\lambda_2}L_\lambda d\lambda \tag{4}$$

Figure 3 shows the designed spectral radiance curve of blue, green, red, and near infrared waveband with Φ800 mm exit port.

The integrated radiance of blue, green, red, and near infrared waveband are listed in Table 1.

Table 2 lists the specification of large aperture integrating sphere.

To ensure the performance of radiation, the built-in light sources were distributed uniformly according to the longitude plane and latitude plane which were near to the exit port. A few experiential combinations have been simulated by tracing 40000000 rays through LightTools [10]. Finally the best combination was generated whose spatial uniformity on 3200 mm × 3200 mm exit port area and angular uniformity at typical positions of the exit port area were relatively good. Figure 4 shows the spatial uniformity simulating figure of 3200 mm×3200 mm exit port and angular

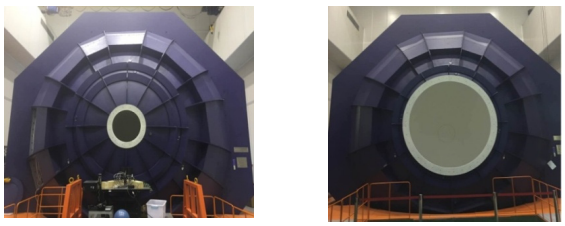

(a) (b)

FIG. 2. (a) Large aperture integrating sphere with Φ800 mm exit port; (b) Large aperture integrating sphere with Φ2500 mm exit port.

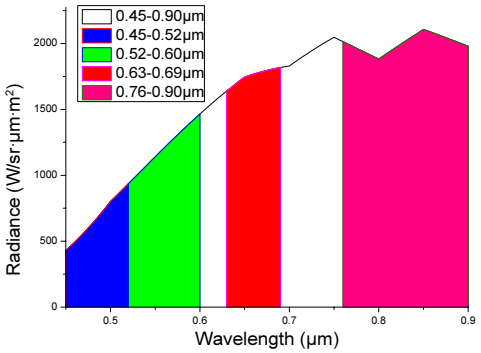

FIG. 3. Spectral radiance of blue, green, red, and near infrared waveband.

TABLE 1. Integrated radiance of blue, green, red, and near infrared waveband

Waveband(μm)	0.45 ~ 0.90	0.45 ~ 0.52	0.52 ~ 0.60	0.63 ~ 0.69	0.76 ~ 0.90
Integrated radiance($W\cdot m^{-2}\cdot sr^{-1}$)	711.44	62.80	96.40	105.29	279.87

TABLE 2. Specification of 8M integrating sphere

Requirement	Specification
Inner diameter	8000 mm
Aperture diameter	800 mm; 2500 mm; 3200 mm
Coating of inner wall	Spectraflect
Sphere coating reflectance (0.3 μm ~1.2 μm)	>96%
Lamp power	80 kw
Lamp type	Tungsten halogen
Color temperature	3000 K
Integrated radiance(0.45 μm ~0.9 μm) for Φ800 mm exit port	> 600 $W\cdot m^{-2}\cdot sr^{-1}$
Internal monitor detector	HR2000+, Si detector
Spatial uniformity (Φ3200 mm exit port)	>95%
Angular uniformity (center position)	>95%

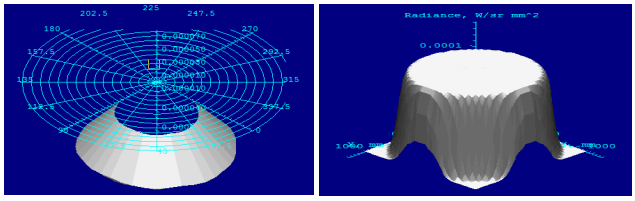

(a) (b)

FIG. 4. (a) Radiation surface figure of angular uniformity at center position by LightTools; (b) Radiation surface figure of spatial uniformity by LightTools.

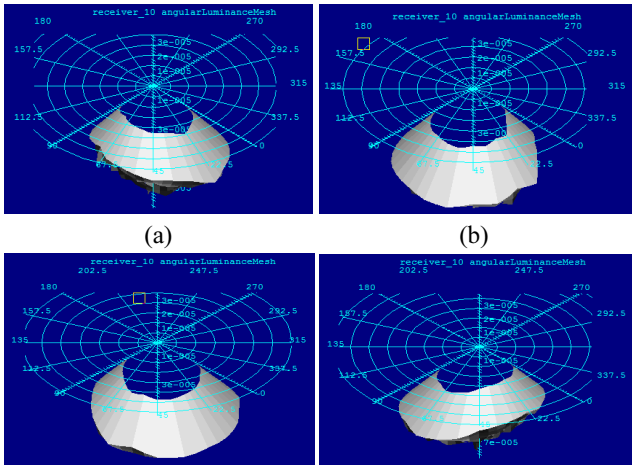

(a) (b)

(c) (d)

FIG. 5. (a) Radiation surface figure of angular uniformity at right edge position by LightTools; (b) Radiation surface figure of angular uniformity at left edge position by LightTools; (c) Radiation surface figure of angular uniformity at top edge position by LightTools; (d) Radiation surface figure of angular uniformity at right down position by LightTools.

uniformity simulating figure of exit port center position. The angular uniformity simulating figure of edge positions is illustrated in Fig. 5. As shown in Fig. 5, there is a radiation drift at the edge of the exit port area. The direction of the drift depends on the simulated position of the exit port. The angular uniformity of center position is about 10% higher than the angular uniformity of edge positions.

Ideally, integrating spheres have good performance of radiation, whose spatial uniformity and angular uniformity are both good. However, it is worth noting that the actual performance of radiation will be influenced by the existence of baffles, the difference between inner light source power, the distribution of inner light sources, and the sphere coating is not an ideal Lambertian emitter. This impact will directly affect the radiometric calibration of remote sensors. Therefore, the radiometric characteristic of the integrating sphere must be measured in practice to confirm the performance of radiation.

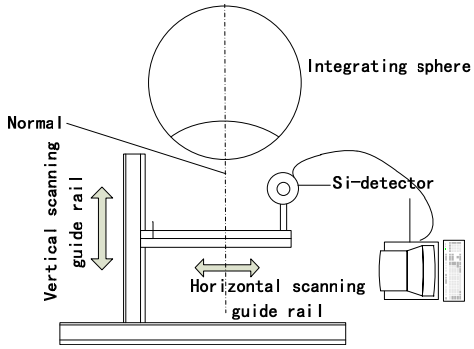

FIG. 6. The single detector method of spatial uniformity measurement.

III. MEASURING THEORY

3.1. Spatial Uniformity Measuring Theory

Spatial uniformity represents the relative standard deviation of radiance from different positions of the exit port area. Generally, a single detector is used to obtain the radiance of the k points. Then the j points of k points are screened out, which are in the range of exit port area. Finally, the spatial uniformity is achieved by the relative standard deviation equation. A Lambertian surface features a radiance that is perfectly diffuse, independent of viewing angle. For the situation of integrating spheres, the radiance of exit port could be calculated by a Lambertian law as shown in Eq. (5).

$$L_\lambda = \frac{\rho_\lambda \times E}{\pi} \tag{5}$$

Hence, spatial uniformity can be obtained by Eq. (6) [11].

$$U_{spatial} = \frac{1}{\overline{L}} \times \sqrt{\sum_{i=1}^{n} (L_i - \overline{L})^2} = \frac{1}{\frac{\overline{E}\rho_\lambda}{\pi}} \times \sqrt{\sum_{i=1}^{n} \left(\frac{E_i \rho_\lambda}{\pi} - \frac{\overline{E}\rho_\lambda}{\pi}\right)^2}$$

$$= \frac{1}{\overline{E}} \times \sqrt{\sum_{i=1}^{n} (E_i - \overline{E})^2} = std(DN_i) / \overline{DN} \times 100\% \tag{6}$$

Where L_i is the radiance of each effective test point I, $\overline{L}$ is the average radiance of test points, E_i is the irradiance of each test point i, $\overline{E}$ is the average irradiance of test points, std (DN_i) is relative standard deviation of DN value of test points, $\overline{DN}$ is the average value of tested points. Hence, the irradiance detector could be used to measure spatial uniformity in practice. Figure 6 shows the working model of the spatial uniformity measuring system based on a single detector.

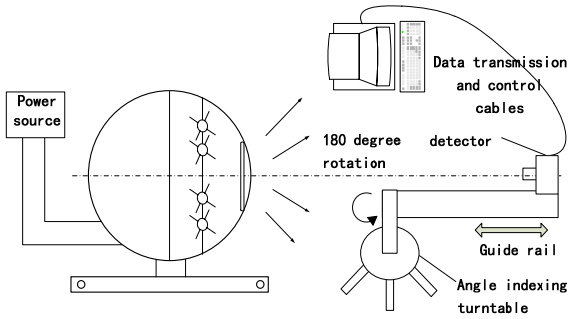

FIG. 7. The single detector method of the angular uniformity measuring system.

3.2. Angular Uniformity Measuring Theory

Angular uniformity represents the relative deviation of different angles. It is expressed by the relative deviation between multi-angle radiance values and normal radiance value. Generally, a single rotating detector is used to obtain radiance of $\beta°$ angular interval. The range of the test solid angle is -$\alpha°$ to $\alpha°$. Then the angular uniformity is obtained by Eq. (7).

$$u_{angular} = min(\frac{L_{\theta_i}}{L_0}) = min(\frac{DN_{\theta_i}}{DN_0}) \quad (7)$$

Where $L_{\theta i}$ is the radiance of angle θ_i, L_0 is the radiance of 0°. Figure 7 shows the working model of the angular uniformity measuring system based on a single detector.

3.3. Restriction of the single detector measurement

Traditional measuring systems are provided with a single detector to scan area or angles. The spatial uniformity measuring device uses a single detector to scan a two-dimensional surface of the test area. The angular uniformity measuring device uses a single luminance detector (with lens) with three degrees of freedom to test radiance of different angles. The single detector method could get good results with small integrating spheres. However, if the diameter increases, longer time will be taken to finish the whole measurement. Longtime power-on will affect the radiation performance of the sphere coating, the service life of inner light sources, and the reliability of the inner light sources. The output radiance will be changed in the situation of longtime power-on. Sequentially, errors will be introduced in the measurement of spatial uniformity and angular uniformity.

IV. DESIGN OF MEASURING SYSTEM

In this paper, a new measuring system consists of multi-detectors, long scanning range, and multiple measuring angles have been developed. Here, they will be divided into two parts: the spatial uniformity measuring device and the angular uniformity measuring device

4.1. Spatial Uniformity Measuring Device

The spatial uniformity measuring device consists mainly of horizontal and vertical scanning guide rail, scanning motor, test frame, and 10 vertical regular interval irradiance Si-detectors. Figure 8 shows the structure of the device.

The interval of 10 vertical irradiance detectors is 320 mm, vertical shifting distance is 500 mm, and the total length of the vertical test frame is 2880 mm. Consequently, the total vertical scan distance is 3380 mm. Before measurement, the optical axis of the detector was put perpendicular to the exit port plane. The irradiance was measured at a selectable interval in horizontal and vertical directions. Finally, two-dimensional plane array points were scanned and tested. The scanning model of the spatial uniformity measuring device is illustrated in Fig. 9. In Fig. 9, the black filled location was the initial position and dotted locations were subsequent scanning positions. The scanning area covered the whole exit port. At one time, radiance of ten vertical regular interval positions was measured whose vertical interval was 320 mm. It tested at one position, then, it moved to the next position and continued testing. Finally, the measured data were recombined according to scanning order, and the

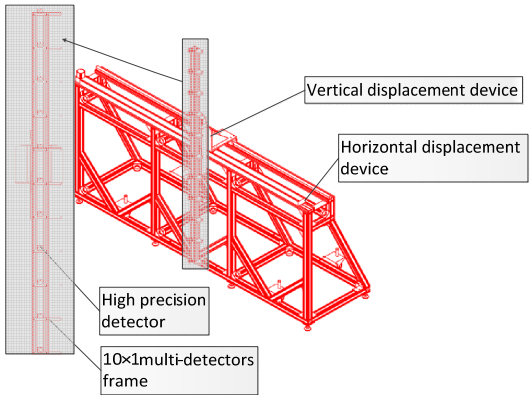

FIG. 8 Structure of the spatial uniformity measuring device.

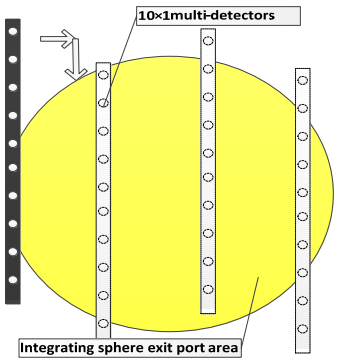

FIG. 9. Scanning model of the spatial uniformity measuring device.

spatial uniformity was calculated by Eq. (6).

4.2. Angular Uniformity Measuring Device

The angular uniformity measuring device consists of horizontal and vertical scanning guide rail, a solid rotation machine, scanning motor, test frame, and 47 regular angular interval radiance Si-detectors. The solid rotation machine is based on strut girder, frame, 47 high-precision radiance Si-detectors, and two-dimensional fine-tuning for each detector. Before measurement, all detectors were ensured to be in the same plane and aligning the same position in the application of two-dimensional fine-tuning. Figure 10 shows the structure of the device.

The vertical shifting distance is 3600 mm and horizontal shifting distance is 3300 mm. The interval of solid rotation tester's detectors is 1.957° in a fixed plane. Hence radiance from -45° to 45° could be measured at a fixed position. The angular interval of the solid rotation machine could be selected from 0.1° to 10°. The schematic diagram of a fixed position test is illustrated in Fig. 11.

Before measurement, the optical axis of the 0° detector was put perpendicularly to the exit port plane at designed distance. Then radiance was measured in the area of the exit port. At each fixed position, the solid rotation machine rotated at a selectable angular interval. The rotating range covered from 0° to 180°. Radiance from -45° to 45° was obtained by 47 radiance Si-detectors at one time. Thus radiance of π space scope was achieved at each fixed position.

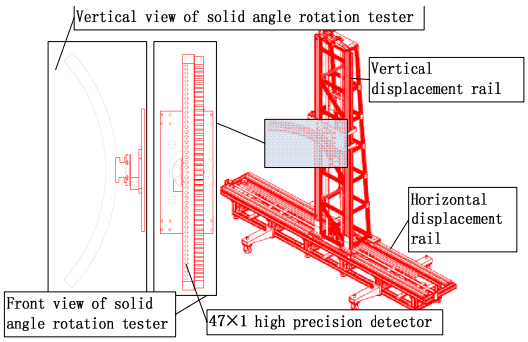

FIG. 10. Structure of the angular uniformity measuring device.

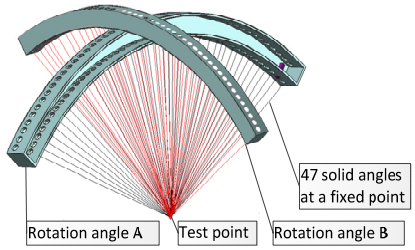

FIG. 11. Principle diagram of the rotation test at a fixed position.

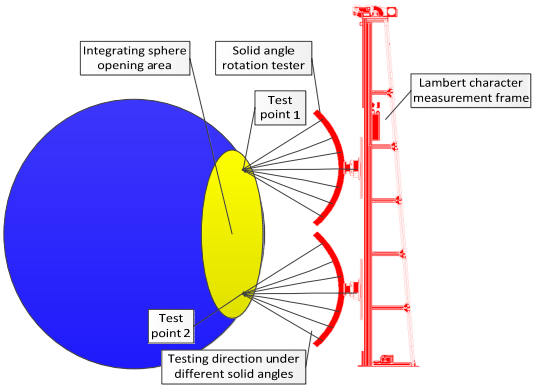

FIG. 12. Scanning model of the angular uniformity measuring device.

Figure 12 shows scanning way of the angular uniformity measuring device. In Fig. 12, the scanning model of the angular uniformity measuring device was similar to the spatial uniformity measuring device. The initial position was test point 1. The solid angle rotation tester measured through the way expounded before. It then moved to test point 2 and continued testing. Finally, the measured data were recombined according to the scanning order. Angular uniformity was calculated by Eq. (7).

4.3. Detector

Irradiance detectors instead of the radiance detectors were used in the spatial uniformity measuring system as explained in Section 3 Subsection 1. The detectors installed with aperture diaphragm and field stop were used to measure radiance. The silicon detector is suitable for large area and longtime experiment, which had good stability and linearity.

4.4. Multiple Detectors Consistency Algorithm

The detectors must be calibrated consistent as they were used to measure different areas or angles of exit port at the same time. In this paper, multi-points uniformity correction method was selected to make the detectors consistent. The integrating sphere radiance range was divided into M segments. All detectors were calibrated at the same time. Figure 13 shows the correction scene of detectors. As shown in Fig. 13, the detectors were put on a designed shelf at the center position of the exit port area (300×300 mm) where the performance of spatial uniformity was good.

$V_{j,i}$(j=1,2,⋯,M; i=1,2,⋯N) was achieved by the detectors from 1 to N (N is the number of detectors) at each radiance level L_j. The integrated spectral radiance L_j was obtained by spectroradiometer PR-735. Figure 14 shows the spectral radiance of different radiance levels.

Then integrated spectral radiance L_j was made linearly fitted by $V_{j,i}$. The relationship between L_j and $V_{j,i}$ was

$$L_j = V_{j,i} \times r_i + b_i \tag{8}$$

$$\begin{vmatrix} L_1 \\ \vdots \\ L_M \end{vmatrix} = \begin{vmatrix} V_{1,1} \times r_1 + b_1 \\ \vdots \\ V_{M,1} \times r_1 + b_1 \end{vmatrix} = \ldots = \begin{vmatrix} V_{1,N} \times r_N + b_N \\ \vdots \\ V_{M,N} \times r_N + b_N \end{vmatrix} \quad (9)$$

Where r_i is the response of detector i and b_i is the intercept of detector i. The r_i and b_i for each detector were calculated by Eq. (10) and Eq. (11) (Cramer's rule). Then r_i and b_i were taken into software. Consistency of the spatial uniformity measuring system was 99.69% and the consistency of angular uniformity measuring system was 99.86%.

$$r_i = \frac{(\sum_{j=1}^{M} V_{j,i} \times \sum_{j=1}^{M} L_j^2) - (\sum_{j=1}^{M} L_j \times \sum_{j=1}^{M} L_j \times V_{j,i})}{M \times \sum_{j=1}^{M} L_j^2 - (\sum_{j=1}^{M} L_j)^2} \quad (10)$$

$$b_i = \frac{M \sum_{j=1}^{M} L_j \times V_{j,i} - \sum_{j=1}^{M} L_j \sum_{j=1}^{M} V_{j,i}}{M \sum_{j=1}^{M} L_j^2 - (\sum_{j=1}^{M} L_j)^2} \quad (11)$$

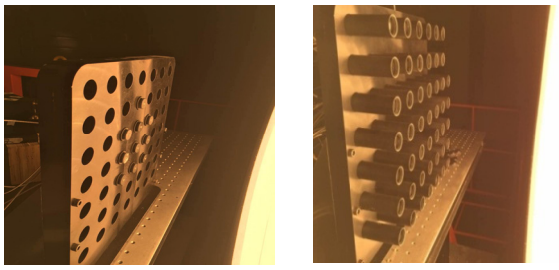

(a) (b)

FIG. 13. (a) Consistency calibration scene of spatial uniformity measuring device; (b) Consistency calibration scene of angular uniformity measuring device.

Table 3 lists the component, function, and parameters of measuring systems.

V. EXPERIMENT

5.1. Spectral Radiance Experiment

Spectroradiometer PR-735 was used to obtain the spectral radiance of exit port Φ800 mm. Figure 15 shows the radiance in the waveband 0.45~0.90 μm with Φ800 mm exit port. The integrated radiance was calculated by Eq. (4).

Table 4 lists the value of theoretical integrated radiance

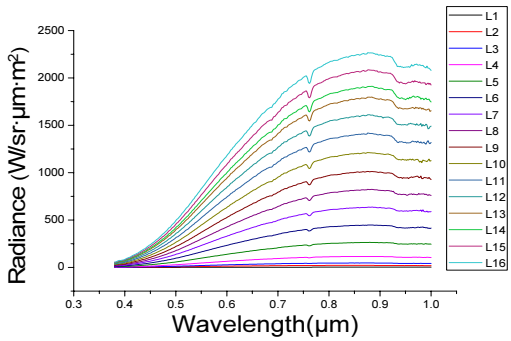

FIG. 14. Spectral radiance of different radiance levels.

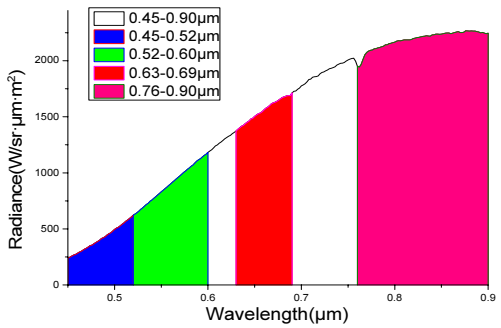

FIG. 15. Tested radiance by the PR-735.

TABLE 3. Summary of large aperture integrating sphere measuring systems

Component	Device	Function	Parameter
Scan device	Spatial uniformity measuring system	Two freedom scan	Scan range：3300×3380 mm Scan speed：0.5 ~ 120 mm/s
	Angular uniformity measuring system	Three freedom scan	Scan range：3300×3600 mm Scan speed：1 ~ 63.75 mm/s Angle scan rate：0.1 ~ 6.375°/s
Detector element	Si irradiance and radiance detector	Radiation detection	Detector stability：≤0.05%/h Detector repeatability：<0.05%
	Data collector	Detector data collection	DC voltage accuracy：0.003% Stability：0.004%/year
Control system	Electric machine control	Scanning point control	Control shaft：A、B、C Communication port：RS232

TABLE 4. Designed and actual integrated radiance of different wavebands

Waveband (μm)	0.45 ~ 0.90	0.45 ~ 0.52	0.52 ~ 0.60	0.63 ~ 0.69	0.76 ~ 0.90
Theoretical integrated radiance($W \cdot m^{-2} \cdot sr^{-1}$)	711.44	62.80	96.40	105.29	279.87
Actual integrated radiance($W \cdot m^{-2} \cdot sr^{-1}$)	671.89	47.59	72.10	93.96	306.56

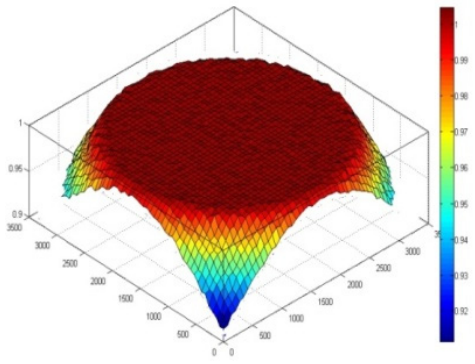

(a)

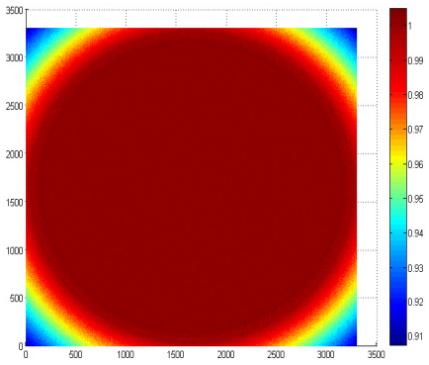

(b)

FIG. 16. (a) Radiation surface 45° view of spatial uniformity; (b) Radiation surface top view of spatial uniformity.

and actual integrated radiance of different wavebands. Due to the difference between designed and actual spectral reflectance, the existence of baffles, and inner sources taking up the coating area, there was a deviation between designed value and actual value.

5.2. Spatial Uniformity Measuring Experiment

320×320 arrays (102400 points) were measured when all tungsten halogen lamps were power-on, whose horizontal interval and vertical interval were 10 mm. The interval of vertical detectors was 320 mm. The whole measurement was finished in less than 2.5 hours. For the single detector method, 28.5 hours would be taken to finish the whole measurement. Hence, in contrast to a single detector method, 9/10 time was saved. Effective data were selected, which were in the exit port area of integrating sphere. Then obtained data were recombined according to the scanning order. The spatial uniformity of Φ3200 mm exit port calculated by Eq. (6) is 98.35% at 100% power. The radiation surface of spatial uniformity is illustrated in Fig. 16. In Fig. 16, the coordinate consists of two-dimensional scan axes (X-Y) and normalized irradiance axis (Z).

5.3. Angular Uniformity Measuring Experiment

Radiance was measured whose rotating angular interval was 2°, and solid angular range covered from -45° to 45°. Radiance of 4230 (90×47) different angles was measured at each fixed position in less than 1.5 minutes. For the single detector method, 70.5 minutes would be taken to finish a fixed position measurement. Hence, in contrast to a single detector method, 46/47 time was saved. The obtained data were recombined according to angular scanning order. The angular uniformity at the center position calculated by Eq. (7) is 98.78%. Figure 17 shows the radiation surface figure of angular uniformity. Figure 18 shows angular uniformity at edge positions. In Fig. 18, the polar coordinate is used

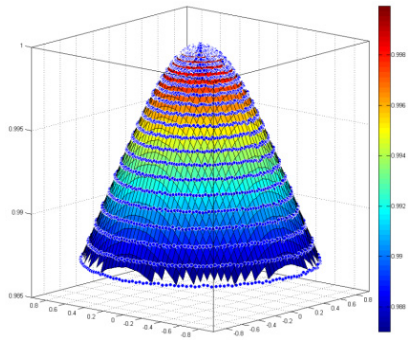

(a)

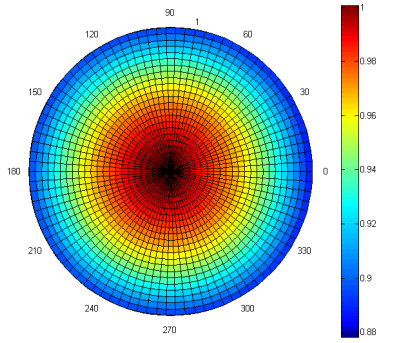

(b)

FIG. 17. (a) Radiation surface side view of angular uniformity at center position; (b) Radiation surface top view of angular uniformity at center position.

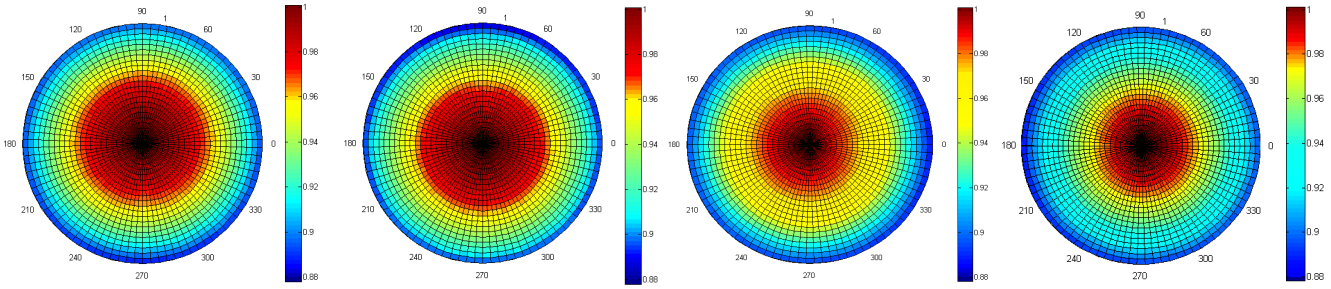

(a) (b) (c) (d)

FIG. 18. (a) Radiation surface figure of angular uniformity at top edge position; (b) Radiation surface figure of angular uniformity at down edge position; (c) Radiation surface figure of angular uniformity at left edge position; (d) Radiation surface figure of angular uniformity at right edge position.

TABLE 5. Results of the spatial uniformity.

Radius (mm)	800	1000	2000	2500	3200
Spatial uniformity	99.684%	99.412%	98.937%	98.676%	98.351%

TABLE 6. Results of the angular uniformity

Position	Center point	Left edge point	Right edge point	Top edge point	Down edge point
Angular uniformity of ±45°	98.78%	88.16%	88.31%	88.65%	88.27%

to indicate the radiation surface whose polar angle direction (φ) represents the rotation direction and polar radius (R) direction represents the locations of 47 detectors.

As shown in Fig. 18, there is a radiation drift at the edge positions of the exit port which is the same as the result of the simulation trend by LightTools in Section 2.

Table 5 lists the data result of spatial uniformity.

Table 6 Data result of angular uniformity.

VI. UNCERTAINTY ANALYSIS

The characteristic of spatial uniformity and angular uniformity is the direct evaluation of the integrating sphere. Hence the measuring uncertainty is required to be analyzed. From Eq. (6) and Eq. (7), the position precision of the scanning device and the uncertainty of the angular rotation tester could be ignored. Before measurement, the consistency algorithm was used to calibrate all detectors. Therefore, the inconsistency of detectors was considered. Besides, the stability of the detector, the uncertainty of the data collector, and the stray light effect should be taken into account. In conclusion, the uncertainty of the system mainly includes the following aspects: (1) Stability of the detector (δ_1); (2) Uncertainty of the data collector (δ_2); (3) Inconsistency of detectors (δ_3); (4) Stray light effect (δ_4). Firstly, the stability experiment was taken to acquire the stability of the detectors. The result indicates that the detector's stability is 0.005% in 12 hours. Secondly, the uncertainty of the data collector was obtained by the repeat test, whose result is 0.004% in 50001 times. Thirdly, the inconsistency of detectors was explained in 4.4. The inconsistency results are 0.31% and 0.14%, respectively. Finally, all optical tables and materials were made in black to reduce the stray light effect to 0.1%. The total uncertainty was calculated by Eq. (12). The uncertainty sources of spatial uniformity measuring system and angular uniformity measuring system are listed in Table 7 and Table 8.

TABLE 7. Uncertainty of spatial uniformity measuring system

Uncertainty sources	Uncertainty (%)
Stability of the detector	0.005
Uncertainty of the data collector	0.004
Inconsistency of detectors	0.310
Stray light effect	0.100
Total uncertainty	0.326

TABLE 8. Uncertainty of angular uniformity measuring system

Uncertainty sources	Uncertainty (%)
Stability of the detector	0.005
Uncertainty of the data collector	0.004
Inconsistency of detectors	0.140
Stray light effect	0.100
Total uncertainty	0.172

$$\delta = \sqrt{\delta_1^2 + \delta_2^2 + \delta_3^2 + \delta_4^2} \tag{12}$$

According to the uncertainty Eq. (12), the total uncertainty (δ) is

$$\begin{aligned}\delta &= \sqrt{\delta_1^2 + \delta_2^2 + \delta_3^2 + \delta_4^2} \\ &= \sqrt{0.005^2 + 0.004^2 + 0.31^2 + 1^2} / 100 = 0.326\%\end{aligned} \tag{13}$$

According to the uncertainty Eq. (12), the total uncertainty (δ) is

$$\begin{aligned}\delta &= \sqrt{\delta_1^2 + \delta_2^2 + \delta_3^2 + \delta_4^2} \\ &= \sqrt{0.005^2 + 0.004^2 + 0.14^2 + 0.1^2} / 100 = 0.172\%\end{aligned} \tag{14}$$

VII. CONCLUSION

An 8000 mm inner diameter large aperture integrating sphere with a variable exit port was designed and manufactured in this paper. The maximum diameter of the exit port is 3200 mm. This integrating sphere will be used for radiometric calibration of the remote sensors with property of wide FOV, large aperture, and long focal length. The simulation for the spatial uniformity and angular uniformity of the output radiance by LightTools is discussed. The best combination of inner light sources was selected by simulation. Integrating sphere design theory and blackbody theory used to design the spectral radiance are explained. Spectral experiment conjugated with spectroradiometer PR-735 was used to verify the designed spectral radiance. With the exit port diameter becoming much larger, a new measurement method was developed which could improve measuring efficiency, save measuring time, protect inner light sources and sphere coating, and improve the measuring accuracy. In contrast to the single detector method, the measuring efficiency of spatial uniformity measuring system was increased by 10 times, and the measuring efficiency of the angular uniformity measuring system was increased by 47 times. Compared to the single detector method, it has the advantage of high efficiency, long scanning range, multi-angle scanning, and good repeatability. The consistency algorithm used to make all detectors consistent is described. From the results of the experiment, the spatial uniformity value is 98.35% and angular uniformity value of the center position is 98.78%. The research we have done suggests an increase in the measuring efficiency of the large aperture integrating sphere. With high measuring efficiency, labor and time costs have been saved, and the effects of longtime source power-on were reduced. The systems have been used to measure a few large aperture uniform source systems and have shown good performance.

ACKNOWLEDGMENT

This work is funded by the National High Technology Research and Development Program of China (863Program) (No. 863-2-5-1-13B)

REFERENCES

1. W. B. Steven, P. E. George, and R. L. Keith, "Facility for spectral irradiance and radiance responsivity calibrations using uniform sources," Appl. Opt. **45**, 8218-8237 (2006).
2. H. P. Wu, Y. W. He ,C. D. Zheng, G. J. Feng, C. Chen, W. Dong, P. Li, and Y. Wang, "Design and characterization of a large aperture spectral radiance source integrating sphere for calibration of satellite remote sensors," Proc. SPIE. **9282**, 928226 1-7 (2014).
3. Y. Y. Lin, G. J. Hong, W. Qun, H. H. Jiang, T. Y. Zhang, and C. Wang, "A design of mid-wave infrared integral catadioptric optical system with wide FOV," J. Opt. Soc. Korea **17**, 142-147 (2013).
4. J. Q. Zhu, W. Sha, C. Z. Chen, X. X. Zhang, and J. Y. Ren, "Integrated modeling for the design of deformable mirrors using a parametric module method," J. Opt. Soc. Korea **19**, 521-530 (2015).
5. Z. Chen, J. Q. Zhu, J. T. Peng, X. X. Zhang, and J. Y. Ren, "A coaxial and off-axial integrated three-mirror optical system with high resolution and large field of view," J. Opt. Soc. Korea **20**, 94-100 (2016).
6. P. Xie, H. Y. Wu, X. B. Zheng, and P. Zou, "Automatic directional radiometric testing system for large aperture integrating spheres," Opt. Precision Eng. **18**, 1943-1950 (2010).
7. Y. S. Zhi, S. T. Chang, and W. Zhu, "Radiometric calibration method for large aperture infrared system with broad dynamic range," Appl. Opt. **54**, 4659-4666 (2015).
8. Y. W. He, P. Li, J. F. Guo, Y. Wang, Z. L. Liu, D. Z. Chun, and P. W. Hou, "Design and characterization of a large-area integrating sphere uniform radiation source for calibration of satellite remote sensors," Proc. SPIE **7656**, 76562 E1-E10 (2010).
9. G. Mckee, S. Pal, H. Seth, A. Bhardwaj, and H. Sahoo, "Design and characterization of a large area uniform radiance source for calibration of a remote sensing imaging system," Proc. SPIE **6677**, 667706 1-9 (2007).
10. H. X. Liu, J. W. Ren, X. S. Li, Z. Wan, Z. L. Xun, B. Y. Li, and J. X. Sun, "Radiometric characteristics simulation of large aperture integrating sphere based on LightTools," Infrared Laser. Eng. **42**, 960-965 (2013).
11. L. Hanssen and A. Prokhorov, "Numerical modeling of an integrating sphere radiation source," Proc. SPIE **4775**, 106-118 (2002).